ACS APPLIED MATERIALS & INTERFACES

Research Article

www.acsami.org

Branch-like Hierarchical Heterostructure (α-Fe_2O_3/TiO_2): A Novel Sensing Material for Trimethylamine Gas Sensor

Zheng Lou, Feng Li, Jianan Deng, LiLi Wang, and Tong Zhang*

State Key Laboratory on Integrated Optoelectronics, College of Electronic Science and Engineering, Jilin University, Changchun, Jilin, 130012 PR China

ABSTRACT: A novel hierarchical heterostructure of α-Fe_2O_3 nanorods/TiO_2 nanofibers with branch-like nanostructures was fabricated using a simple two-step process called the electrospinning technique and hydrothermal process. A high density of α-Fe_2O_3 nanorods (about 200 nm in diameter) was uniformly deposited on a TiO_2 nanofibers backbone. The phase purity, morphology, and structure of hierarchical heterostructures are investigated by X-ray diffraction (XRD), field emission scanning electron microscopy (FESEM), transmission electron microscopy (TEM), and energy-dispersive X-ray (EDX) analysis. The highly branched α-Fe_2O_3/TiO_2 heterostructures provided an extremely porous matrix and high specific surface area required for high-performance gas sensors. Different nanostructured α-Fe_2O_3/TiO_2 heterostructures are also investigated by controlling the volume ratio of the reactants. The α-Fe_2O_3/TiO_2 heterostructures with a proper mixture ratio of the reactants sensor exhibit obviously enhanced sensing characteristics, including higher sensing response, lower operating temperature, faster response speed, and better selectivity in comparison with other ones. Moreover, the α-Fe_2O_3/TiO_2 heterostructures sensor also exhibits excellent sensing performances compared with α-Fe_2O_3 nanorods and TiO_2 nanofibers sensors. Thus, the combination of TiO_2 nanofibers backbone and α-Fe_2O_3 nanorods uniformly decorated endows a fascinating sensing performance as a novel sensing material with high response and rapid responding and recovering speed.

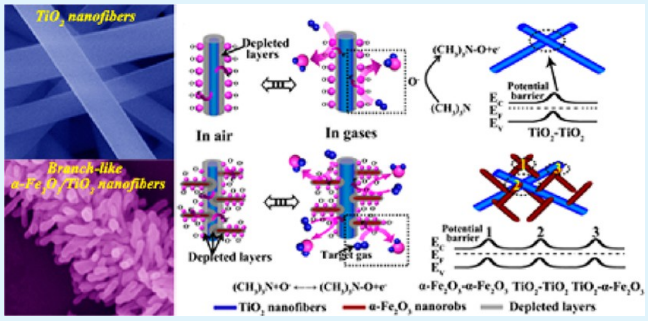

KEYWORDS: *α-Fe_2O_3/TiO_2, hierarchical heterostructures, TMA sensing, high response*

1. INTRODUCTION

Recently, a one-dimensional (1D) semiconducting metal oxide nanostructure has been the focus of further study because of their novel properties and wide use in optics, electronics, gas sensors, and so on.[1−5] In particular, metal oxides (In_2O_3, SnO_2, and TiO_2 nanowires) due to their attractive electrical and optical properties have been extensively researched in the gas sensing field.[6−8] Although exciting results have been reported, for the sensors based on 1D nanostructures, the challenge to improve the sensitivity and selectivity still exists. Nowadays, several methods have been concentrated on for improving their response and selectivity, including noble metal functionalization, element doping, photoluminescence, and other metal oxides loaded onto support material formed heterostructure constructing.[9−15] Actually, branched 1D nanostructures assembly of nanoscale building blocks with a tunable dimension and structure complexity provide both large specific surface materials and multifunctional nanomaterials.[16]

Branched 1D heterostructures composed of stem 1D nanomaterials and grown branch 1D nanomaterials have been widely used due to their fascinating physical and chemical properties, such as solar cell,[17] photodetectors,[18] and field electron emission.[19,20] However, branched 1D nanomaterials used in gas sensors have rarely been investigated. As an application of gas sensor, Kim has reported four mechanisms of stem-branch heterostructure to provide improved sensing properties. Importantly, when stem-branch heterostructured nanowires are exposed to target gas molecules, the change in conductance of stem-branch nanostructures will be greater.[21] During the past years, composite nanostructures, which were combined by α-Fe_2O_3 and TiO_2, such as composite nanoparticles,[22] composite nanotubes,[23] and core−shell nanostructures,[24] have been reported. A good ethanol-sensing performance of α-Fe_2O_3/TiO_2 tube-like nanostructures has been investigated.[25] Otherwise, the improved gas-sensing properties may be due to the heterojunction formed at interface of the α-Fe_2O_3 and TiO_2 nanostructures which can improve the surface-depletion effect more easily. However, there still is a challenge to develop an efficient way for the controllable synthesis of branched-like α-Fe_2O_3/TiO_2 heterostructures. Clearly, it is necessary to carry out further studies in this area.

In our work, we report an effective two-step route to synthesize branched 1D α-Fe_2O_3/TiO_2 heterostructures by a combination of the electrospinning and hydrothermal method. First, we introduced an electrospinning technique to prepare TiO_2 nanofibers as substrates. Subsequently, α-Fe_2O_3 nanorods

Received: June 28, 2013
Accepted: October 8, 2013
Published: October 8, 2013

   dx.doi.org/10.1021/am402532v | *ACS Appl. Mater. Interfaces* 2013, 5, 12310−12316

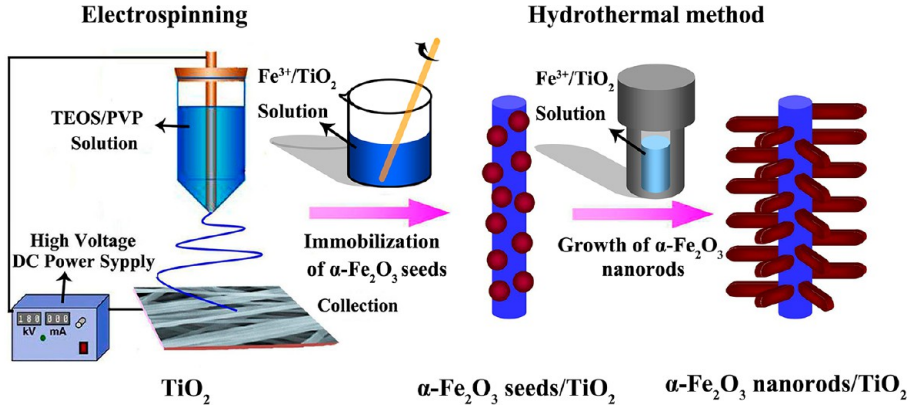

Figure 1. Synthesis strategy to branch-like α-Fe_2O_3/TiO_2 hierarchical heterostructure.

were formed on the TiO_2 fibers through hydrothermal treatment. Excellent trimethylamine (TMA) sensing properties based on α-Fe_2O_3/TiO_2 heterostructures with different molar ratio were investigated. Compared with pristine α-Fe_2O_3 and TiO_2 sensors, the sensors based on α-Fe_2O_3/TiO_2 have higher response and better selectivity to low concentration TMA at 250 °C. Furthermore, the response/recovery speed for our sensors is also much shorter. The excellent sensing performance is probably due to the unique heterostructure of α-Fe_2O_3/TiO_2.

2. EXERIMENTAL SECTION

2.1. Synthesis Process. The purity of all chemicals was of analytical grade, and there is no subsequent purification process. Ferric trichloride, tetrabutyl titanate, ammonia, glacial acetic, and poly-(vinlypyrrolidone) were purchased from Sinopharm. The experimental procedure is shown in Figure 1.

Preparation of TiO_2 Nanofibers. TiO_2 nanofibers were synthesized following our group's reported literature;[26] 2 g of tetrabutyl titanate and 2 g of glacial acetic were added to 7.5 g of ethanol. In addition, 11.5 wt % of poly-(vinlypyrrolidone) (PVP) solution was introduced into the above solution under vigorous stirring. After 4 h of stirring at room temperature, mixed solution was transferred into a syringe for electrospinning and the applied electric voltage was 20 kV. Composite PVP/tetrabutyl titanate nanofiber film was annealed at 500 °C (2 h) for removing polymer and impurities. Finally, The TiO_2 nanofibers were obtained.

Preparation of α-Fe_2O_3 Nanorods. $FeCl_3{\cdot}6H_2O$ (0.844 g) was dispersed in a mixture with 20 mL of deionized water and 0.05 mL of ammonia under ultrasonication (30 min). The final mixture was transferred into a 40 mL Teflon-lined autoclave and heated hydrothermally at 95 °C for 4 h. The products were harvested via centrifugation six times with ethanol and water. After drying at 60 °C for 24 h, the products with a dark-red color were annealed to 500 °C (2 h) in the muffle furnace (heating rate of 5 °C min^{-1}).

Preparation of α-Fe_2O_3/TiO_2 Heterostructures. α-Fe_2O_3 nanorod depositions were fabricated by the modified literature method.[27] Briefly, 0.844 g of $FeCl_3{\cdot}6H_2O$ was first dissolved in 20 mL of deionized water and 0.05 mL of ammonia under continuously stirring. TiO_2 nanofibers (0.01 g) were put into the solution. The obtained solution was transferred into a Teflon-lined autoclave with volume of 40 mL. The Teflon-lined autoclave was sealed and heated at 95 °C for 4 h and cooled to room temperature. The film was collected and washed with ethanol and deionized water, respectively. After drying at 60 °C for 24 h, the products were annealed to 500 °C (2 h) in the muffle furnace. Three other types of α-Fe_2O_3/TiO_2 samples are prepared for comparison with a similar method. The preparation process of four α-Fe_2O_3/TiO_2 materials is summarized in Table 1.

2.2. Characterization. The crystalline phase of all α-Fe_2O_3/TiO_2, α-Fe_2O_3, and TiO_2 products were examined via X-ray diffraction (XRD, Rigaku D/Max-2550, λ = 0.154 18 nm), and surface structure, size, and so on were determined by field emission scanning electron microscopy (FESEM) from SHIMADZU Japan (SSX-550) with energy-dispersive X-ray (EDX), Brunauer–Emmett–Teller (BET), and transmission electron microscopy (TEM), respectively.

Table 1. Detailed Experimental Parameters (Material, Temperature, Time, and so on) for the Preparation of Four α-Fe_2O_3/TiO_2 Samples[a]

sample no.	starting reagents	hydrothermal temperature and time	morphology
S-1	0.135 (±0.001) g $FeCl_3{\cdot}6H_2O$ + 0.05 mL NH_3 + 20 mL H_2O + 0.01 g TiO_2	95 °C 4 h	nanofibers
S-2	0.338 (±0.001) g $FeCl_3{\cdot}6H_2O$ + 0.05 mL NH_3 + 20 mL H_2O + 0.01 g TiO_2	95 °C 4 h	nanofibers
S-3	0.844 (±0.001) g $FeCl_3{\cdot}6H_2O$ + 0.05 mL NH_3 + 20 mL H_2O + 0.01 g TiO_2	95 °C 4 h	branch-like nanofibers
S-4	1.351 (±0.001) g $FeCl_3{\cdot}6H_2O$ + 0.05 mL NH_3 + 20 mL H_2O + 0.01 g TiO_2	95 °C 4 h	branch-like nanofibers

[a]All samples were annealed at 500 °C for 2 h.

2.3. Fabrication and Measurement of Gas Sensor. First, a sensing paste is mainly composed of as-obtained branch-like α-Fe_2O_3/TiO_2 hierarchical structure and deionized water in an agate mortar (weight ratio 4:1). Second, the obtained paste used as sensitive body was coated on a ceramic tube with two gold electrodes and platinum wires. Figure 2a shows a diagram of the α-Fe_2O_3/TiO_2 sensor. A Ni–Cr heating wire was placed inside the component as a resistor to adjust the whole working temperature of gas sensors. Figure 2b shows the working principle of the sensors. The sensor export voltage was tested by using a common electrical circuit with voltage of 5 V (V_S).

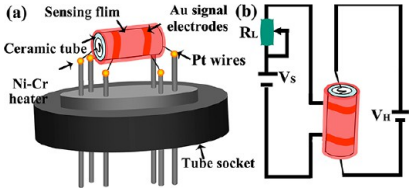

Figure 2. (a) Schematic of the α-Fe_2O_3/TiO_2 heterostructure sensor. (b) Circuit diagram of the test system.

The sensing performances of three samples were characterized by an Intelligent Test system (RQ-2, China). When putting the sensors in a closed glass chamber, the measurement of the sensitive performance was operated by injecting an appropriate amount of target gases. The

corresponding gases were prepared from appropriate liquid; different gas concentrations in the glass chamber were calculated by a formula. More details regarding the formula are provided in the literature.[28] The response is ratio of resistances in air and gas ($S = R_a/R_g$). The response/recovery time (T_{r1}/T_{r2}) was described as the time in which the resistance changes to 90%. More details of gas sensing experiments are in our previous work.[29]

3. RESULTS AND DISCUSSION

3.1. Composition and Structure. The crystallographic information associated with α-Fe_2O_3 nanorods, TiO_2 nanofibers, and α-Fe_2O_3/TiO_2 heterostructures has been investigated by XRD, as illustrated in Figure 3. Compared with the

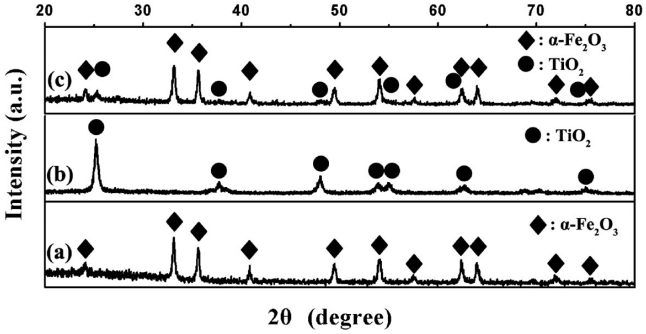

Figure 3. XRD pattern of (a) α-Fe_2O_3 nanorods, (b) TiO_2 nanofibers, and (c) α-Fe_2O_3/TiO_2 heterostructures, respectively.

data in α-Fe_2O_3 JCPDS card (No. 33-0664) and TiO_2 JCPDS card (No. 21-1272), Figure 3a,b shows all the diffraction peaks can be indexed as hematite α-Fe_2O_3 and anatase TiO_2. Figure 3c shows two mixed phases of hematite α-Fe_2O_3 and anatase TiO_2. The rhombus indicates the peaks coming from hematite α-Fe_2O_3 (JCPDS No. 33−0664), while the others come from anatase TiO_2 (JCPDS No. 21-1272). No other impurity diffraction peaks are discovered, which confirm the purity of the product. For this point, the materials not only are process perfect crystalline phases but also maintain original physical structure. Thus, it is confirmed that the materials formed a nanocomposite rather than alloy.

Figure 4 shows FESEM micrographs of α-Fe_2O_3/TiO_2 heterostructures with different magnification after hydrothermal

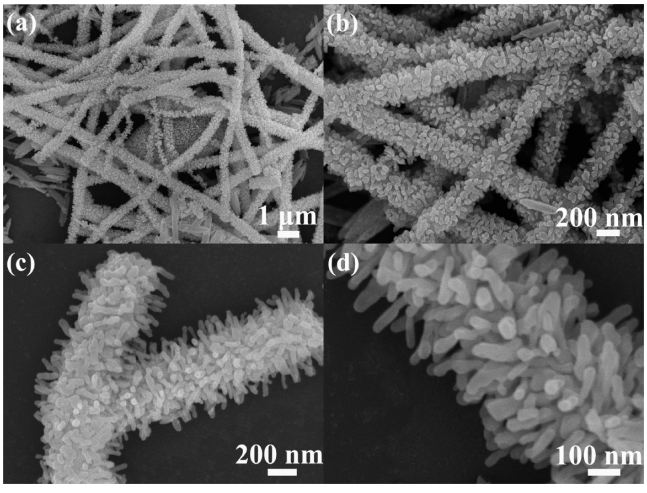

Figure 4. FESEM images of the α-Fe_2O_3/TiO_2 heterostructures: (a,b) panoramic and (c,d) magnified.

treatment at 95 °C for 4 h. It can be observed from Figure 4a,b that the products are mainly composed of branch-like nanofibers with average diameter of about 600 nm. The high-magnification FESEM image (Figure 4c) shows that the branch-like α-Fe_2O_3/TiO_2 heterostructure possess rough and well-aligned surfaces, which are built up from compactly aggregated irregular-shaped α-Fe_2O_3 nanorods. Moreover, an individual branch-like α-Fe_2O_3/TiO_2 heterostructure with a loose and rough surface is shown in Figure 4d. This hierarchical branch-like α-Fe_2O_3/TiO_2 may apply to a gas sensor due to these rough, loose, and well-aligned surfaces, including the stem and branch parts of branch-like heterostructures, compared to that of the individual components nanostructures.

For comparison, the structures of the prepared TiO_2 and α-Fe_2O_3 products were also investigated as shown in Figure 5. It

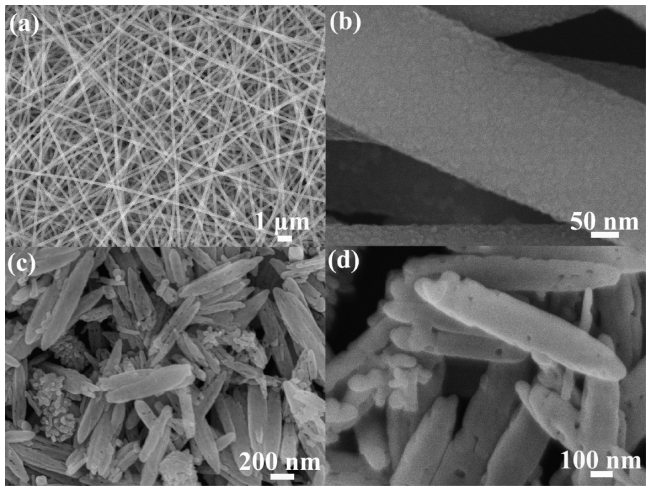

Figure 5. FESEM images of (a,b) the TiO_2 nanofibers and (c,d) the α-Fe_2O_3 nanorods.

can be seen from Figure 5a,b that the surface of pristine TiO_2 nanofibers is relatively smooth with about 200 nm in diameter. In addition, Figure 5c,d shows α-Fe_2O_3 nanorods have an approximately uniform morphology with the diameter and length of 100−300 nm and 1 μm, respectively.

Transmission electron microscopy (TEM) provides insights into the structure of TiO_2 nanofibers, α-Fe_2O_3 nanorods, and branch-like α-Fe_2O_3/TiO_2 heterostructures. Figure 6a,b shows the TEM image of the initial TiO_2 nanofibers, where the prepared TiO_2 nanofibers appear to be smooth on the surface without α-Fe_2O_3 nanorods. Figure 6c,d presents the TEM image of α-Fe_2O_3 nanorods obtained after hydrothermal treatment at 95 °C for 4 h. One can notice that the sample was composed of nanorods with a mean size of 100−300 nm. Figure 6e shows that α-Fe_2O_3 nanorods have been densely grown on the TiO_2 nanofibers after the hydrothermal process. With more details shown in Figure 6f, the results reveal that the size of α-Fe_2O_3 nanorods is consistent with that shown in Figure 4 and the surfaces of each branch-like heterostructure are very loose. These networks are inferred to be beneficial for the gas sensors, due to the rapid and effective gas diffusion between inward and outward. The scanning SEM (SSEM) image shows a single α-Fe_2O_3/TiO_2 heterostructure, combined with EDX elemental mapping (Figure 6g−j), which confirms that the heterostructures have been formed between the TiO_2 nanofibers and α-Fe_2O_3 nanorods after the hydrothermal

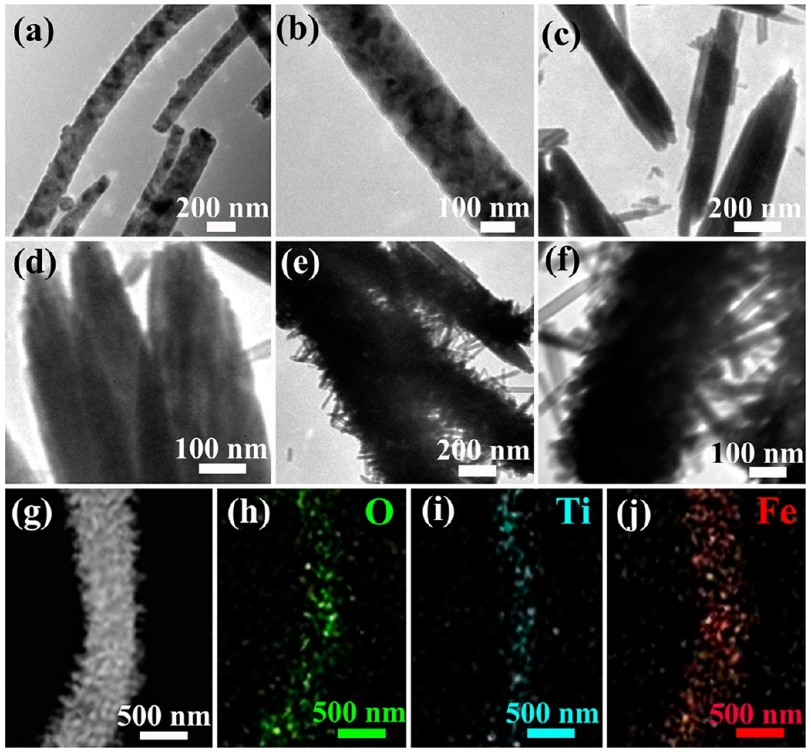

Figure 6. TEM images of (a,b) the TiO_2 nanofibers and (c,d) the α-Fe_2O_3 nanorods; (e,f) TEM images of α-Fe_2O_3/TiO_2 heterostructures; (g) the SSEM image of α-Fe_2O_3/TiO_2 heterostructures; (h–j) EDX elemental mappings of O, Ti, and Fe, respectively.

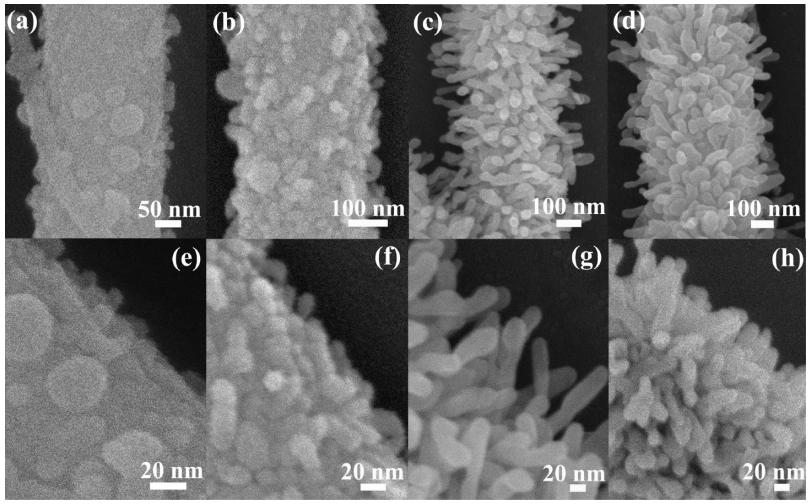

Figure 7. FESEM images of hierarchical α-Fe_2O_3/TiO_2 heterostructures with different molar ratio: (a,e) S-1, (b,f) S-2, (c,g) S-3, and (d,h) S-4.

process. This data also reveals that the branch-like heterostructures are composed of three elements: O, Ti, and Fe.

Figure 7 shows the structures of the products with different molar ratio of the $FeCl_3 \cdot 6H_2O$ to TiO_2 nanofibers in the precursor solution. It can be found that the surfaces of all samples turns coarser compared with the pristine TiO_2 nanofibers, which can be attributed to the successful growth of the secondary α-Fe_2O_3 nanoparticles on the primary TiO_2 substrates. Moreover, control of structure and coverage density of secondary α-Fe_2O_3 materials was achieved by tuning the concentration of precursor (Fe^{3+}). When the molar ratio of the $FeCl_3 \cdot 6H_2O$ to TiO_2 nanofibers in the precursor solution is increased to 4: 1 (S-1), it can be observed (Figure 7a,e) that many nanoparticles with an diameter of 10–20 nm are formed on the surface of the TiO_2 nanofibers. However, as the molar ratio is increased to 10: 1 (S-2), it can be seen that the aggregation phenomenon occurred and many nanoparticles transformed into obviously small nanorods with coarse surfaces (Figure 7b,f). When the molar ratio is increased to 25:1 (S-3), the second α-Fe_2O_3 nanorods appear and cover the TiO_2 nanofibers used as the backbone (Figure 7c,g). When the molar ratio is increased continuously to 40:1 (S-4), a layer of dense α-Fe_2O_3 nanorods grown on TiO_2 nanofibers is generated (Figure 7d,h).

3.2. TMA Sensing Properties. It is very well-known that examination of fish freshness is one of the most important issues in the fishery business. Trimethylamine (TMA) is in a wide range of animal organs and proteins which is produced in

the course of microbial degradation of trimethylamine N-oxide (TMAO).[30] With the decrease in freshness, TMA gas is gradually increased, so the TMA gas detection has become more and more important in the field of food spoilage due to volatility. Wu has reported that Ru-loaded TiO_2 nanomaterials exhibit a good TMA-sensing; however, high operating temperature is a necessary condition involving higher cost.[31]

Importantly, the operating temperature is closely linked with the response for semiconductor oxide sensors. As shown in Figure 8, the responses of six sensors to 50 ppm TMA were

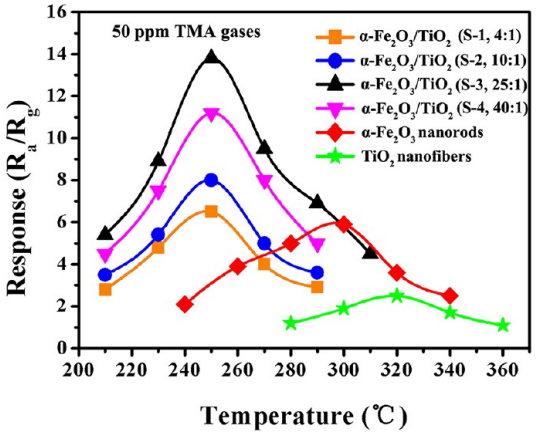

Figure 8. Responses of four α-Fe_2O_3/TiO_2 heterostructures with different molar ratios, pristine α-Fe_2O_3 nanorods, and TiO_2 nanofibers at different operating temperatures, to 50 ppm of TMA, respectively.

measured under different operating temperatures. The response curves showed a parabolic-shape in the entire test range. The maximum response of four α-Fe_2O_3/TiO_2 sensors appearing at 250 °C are (S-1) 6.5, (S-2) 8.0, (S-3) 13.9, and (S-4) 11.2, respectively. Similarly, The maximum response of pristine α-Fe_2O_3 and TiO_2 sensors is 5.9 and 2.3 at 300 and 320 °C, respectively. Compared with all sensors, the highest response was also S-3 sensor (with molar ratio 25:1) at 250 °C. This enhancement in response toward S-3 may contribute to the well-known catalytic activity of α-Fe_2O_3.[32] Most importantly, TiO_2 nanofibers coated with α-Fe_2O_3 nanorods display a lower operating temperature than the pristine α-Fe_2O_3 nanorods and TiO_2 nanofibers.

Figure 9a presents the temporal response/recovery of pristine α-Fe_2O_3, TiO_2, and α-Fe_2O_3/TiO_2 (S-3) sensors to different TMA gas concentrations at 300, 320, and 250 °C, respectively. The sensing responses of α-Fe_2O_3/TiO_2 sensors to 10, 50, 80, 100, and 200 ppm of TMA were 6.8, 13.9, 22.1, 33.1, and 48.6, respectively. This shows that the sensitivity of α-Fe_2O_3/TiO_2 (S-3) sensor increased almost 2−2.5- and 6−16-fold as for pristine ones, which indicated that novel nanostructure and synergistic effect play an essential role to enhance the response of gas sensors. To prevent possible loss and disasters, not only gas response but also response time should be enhanced. In particular, the latter is required for real-time monitoring of toxic and hazardous gases. Figure 9b−d shows the temporal responses of one single period of pristine α-Fe_2O_3, TiO_2, and α-Fe_2O_3/TiO_2 (S-3) to TMA gases at 300, 320, and 250 °C, respectively. It can be observed that the three sensors display fast response/recovery time: 0.5 s/1.5 s (α-Fe_2O_3/TiO_2, S-3), 1 s/2 s (α-Fe_2O_3), and 7 s/12 s (TiO_2) to 50 ppm of TMA, respectively. The comparisons of TMA

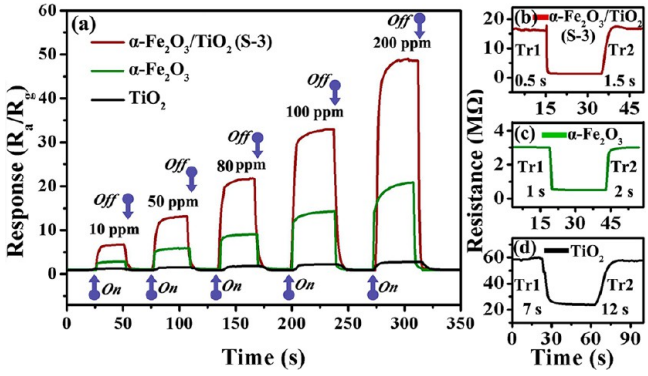

Figure 9. (a) Dynamic TMA-sensing response curves of the pristine α-Fe_2O_3 nanorods, TiO_2 nanofibers, and α-Fe_2O_3/TiO_2 heterostructures; (b−d) response/recovery time of the pristine α-Fe_2O_3 nanorods, TiO_2 nanofibers, and α-Fe_2O_3/TiO_2 heterostructures to 50 ppm TMA.

responses of various compounds nanostructures in the literature were summarized in Table 2.[33−36]

Table 2. Comparison of TMA-Sensing Properties of the Present Results with Reported Results[a]

materials	TMA conc., ppm	temp., °C	response	T_{r1}/T_{r2}, s
this work	50	250	13.9	0.5/1.5
WO_3 sphers[33]	5	450	56.9	1.5/486
ZnO film[34]	400	300	2.8	
WO_3 film[35]	50	70	3	6.5/21
In_2O_3 rod[36]	5	340	5.9	5/10

[a]TMA conc. = TMA gas concentration. Temp. = temperature. T_{r1}/T_{r2} = response/recovery time.

Three sensors' responses as a function of TMA concentrations are illustrated in Figure 10a. The TMA-sensing response of α-Fe_2O_3/TiO_2 (S-3) sensor was linear from 10 to 200 ppm but tends to saturate when TMA concentration increased from 800 to 2000 ppm. These results revealed that our sensors have a strong detection to low concentration TMA gas. Selectivity is the most remarkable aspect of the sensing characteristics. In fact, a sensor with good selectivity can detect a target gas when it was exposed to the multicomponent gas environment, especially with similar physicochemical properties. Figure 10b depicts the histogram of the response of three sensors based on pristine α-Fe_2O_3, TiO_2, and α-Fe_2O_3/TiO_2 (S-3) toward 50 ppm of C_3H_9N (TMA), C_7H_8, HCHO, NH_3, and C_3H_6O, respectively. The response of α-Fe_2O_3/TiO_2 (S-3) sensor to C_3H_9N (TMA) is 2.5−7 times higher than that to other gases including C_7H_8, HCHO, NH_3, and C_3H_6O and is also higher than that of pristine ones. Stability, which is the ability to sequentially respond to the target gas without a visible decrease in sensitivity, is also the key criterion for practical application. Figure 10c illustrates a series of dynamic response of the α-Fe_2O_3/TiO_2 (S-3)-based sensor to 10, 50, and 80 ppm of TMA. It is also found that the on and off responses for the α-Fe_2O_3/TiO_2 (S-3)-based sensor could be repeated and there is no clear change in responses during 3 cycles measurement to 10, 50, and 80 ppm of TMA, revealing excellent stability and reproducibility of the sensor.

3.3. Gas Sensing Mechanism. In the case of specimen α-Fe_2O_3/TiO_2, the sensor exhibits better sensing performance than that of the pristine ones. Otherwise, the work on branch-

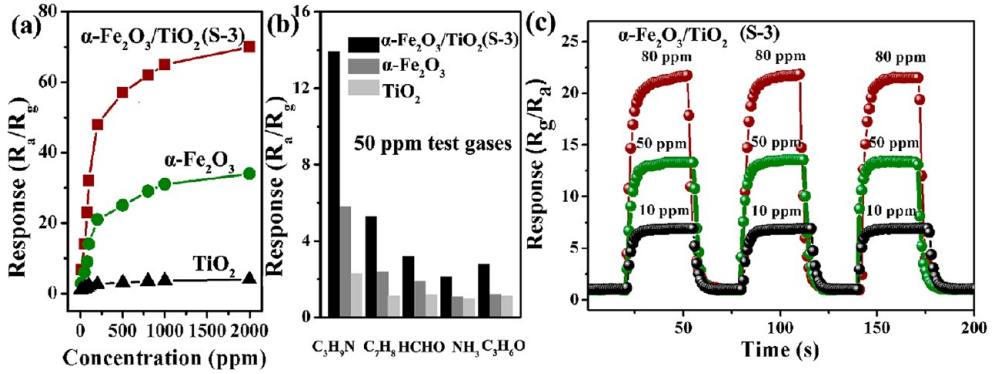

Figure 10. (a) Response of the α-Fe_2O_3 nanorods, TiO_2 nanofibers, and α-Fe_2O_3/TiO_2 heterostructures to 10−2000 ppm of TMA. (b) Selectivity tests of the pristine α-Fe_2O_3 nanorods, TiO_2 nanofibers, and α-Fe_2O_3/TiO_2 heterostructures sensors to 50 ppm of different gases. (c) Reproducibility of the α-Fe_2O_3/TiO_2 sensor upon exposure (3 cycles) to 10, 50, and 80 ppm TMA gas at 250 °C.

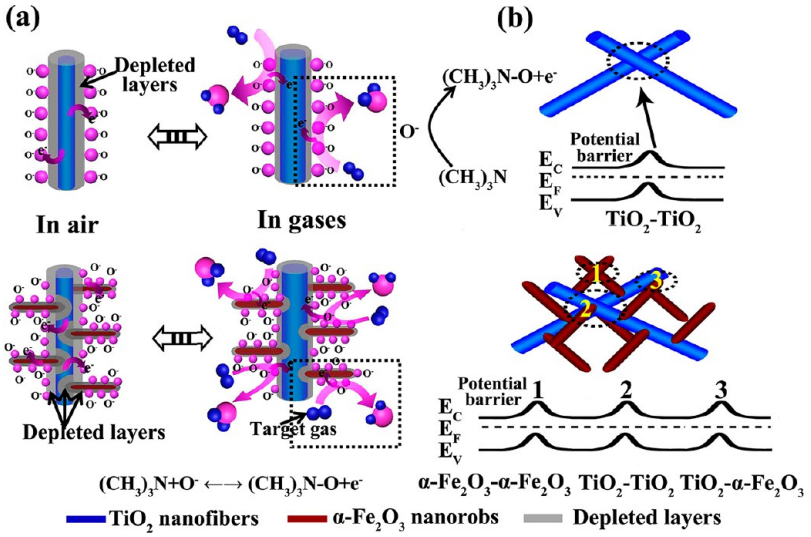

Figure 11. (a,b) Schematic illustration of sensing mechanism of the bare TiO_2 nanofibers and the α-Fe_2O_3/TiO_2 hierarchical heterostructure.

like α-Fe_2O_3/TiO_2 heterostructure TMA sensors has not been reported so far. The branch-like heterostructure nanofibers displaying good gas-sensing performance can use two possible mechanisms. First, it can be explained that α-Fe_2O_3/TiO_2 heterostructure generates an enhanced charge separation at the interface between the α-Fe_2O_3 nanorods and TiO_2 nanofibers, resulting in the enhanced conductance modulation (Figure 11a).[37] In the pristine TiO_2 nanofibers network, the electron depletion layer was formed due to the adsorption of oxygen ions (O^-, O^{2-}, O_2^-), which leads to a decrease in the sensor conductivity (Figure 11a, left). The electron transfer from the adsorbed TMA molecule to the TiO_2 is energetically feasible, as illustrated in Figure 11a, right, resulting in a decrease of electron depletion layer and an increase of the charge-carrier density and thus an increase of the conductivity.[37] After the TiO_2 nanofibers surface was decorated by the α-Fe_2O_3 nanorods, the sensor response to the TMA gas is markedly enhanced, and the gas sensing mechanism is different from that of the pristine TiO_2 sensor, due to the existence of the α-Fe_2O_3 nanorods. The synergistic effect of TiO_2 nanofibers and α-Fe_2O_3 nanorods is a key factor for improving sensing performances. The Schottky barrier and an additional depletion layer between α-Fe_2O_3 nanorods and TiO_2 nanofibers is formed since the work function of α-Fe_2O_3 (5.88 eV)[38] is greater than that of TiO_2 (4.2 eV),[39] making it easy for the electrons in TiO_2 nanofibers to transfer to α-Fe_2O_3 nanorods (Figure 11a). Moreover, the surface area of the α-Fe_2O_3/TiO_2 heterostructure (37 m^2 g^{-1}) is larger than that of the bare TiO_2 nanofibers (21 m^2 g^{-1}) and α-Fe_2O_3 nanorods (7 m^2 g^{-1}), which allows them to absorb more gas molecules. Additionally, the high dispersity of α-Fe_2O_3 nanorods on the surface of TiO_2 nanofibers provides efficient and rapid electron exchange between the cations: Fe(III) ↔ Fe(II).[40] Thus, it can make the conductivity have greater changes and improve the gas sensing performance. For the second possible sensing mechanisms, the potential barriers are formed at junctions between nanofibers, making it modulating for the electrons to travel between adjacent electrodes, with the direction of the electron transfer depending on adsorbing or desorbing gas molecules.[41,42] Compared with the pristine one, the TMA response enhancement of α-Fe_2O_3/TiO_2 hierarchical heterostructure can be due to the presence of α-Fe_2O_3/TiO_2 heterojunctions and α-Fe_2O_3/α-Fe_2O_3 homojunction (Figure 11b). These junctions can be used for additional active sites, leading to improvement of sensing performances.[21,41−43]

4. CONCLUSIONS

In conclusion, we report the synthesis of α-Fe_2O_3/TiO_2 with hierarchical structure by a two-step process with electrospinning and a subsequent hydrothermal process. The as-

prepared α-Fe_2O_3/TiO_2 products display a branch-like nanofiber with the average diameter of about 600 nm. Otherwise, by adjusting the molar ratio of the $FeCl_3 \cdot 6H_2O$ to the TiO_2 nanofibers, different structures and coverage densities of secondary α-Fe_2O_3 materials were obtained. The effects of α-Fe_2O_3 loading on the TiO_2 nanofibers for TMA-sensing properties have been investigated. The sensor based on α-Fe_2O_3/TiO_2 branch-like heterostructures (S-3) provides the response of 13.9 to 50 ppm TMA gas and fast response/recovery rate (0.5 s/1.5 s). The results demonstrate that this hierarchical heterostructure provides a direction for designing high-performance gas sensors.

AUTHOR INFORMATION

Corresponding Author

*E-mail: zhangtong@jlu.edu.cn. Tel.: +86 431 85168385. Fax: +86 431 85168270.

Notes

The authors declare no competing financial interest.

ACKNOWLEDGMENTS

This work was financially supported by the Natural Science Foundation Committee (NSFC, Grant No. 51102109), the program for Chang Jiang Scholars and Innovative Research Team in University (No. IRT1017), and Project of Innovation Research Team of Jilin University (Grant No. 201004003).

REFERENCES

(1) Nixon, G.; Devashankar, S.; Rathnakumari, M.; Sureshku-mar, P. *J. Alloys Compd.* **2010**, *507*, 225−229.

(2) Comini, E.; Faglia, G.; Sberveglieri, G.; Calestani, D.; Zanotti, L.; Zha, M. *Sens. Actuators, B* **2005**, *111*, 2−6.

(3) Wei, S. H.; Yu, Y.; Zhou, M. H. *Mater. Lett.* **2010**, *64*, 2284−2286.

(4) Hernandez-Ramirez, F.; Prades, J. D.; Tarancon, A.; Barth, S.; Casals, O.; Jimenez-Diaz, R.; Pellicer, E.; Rodriguez, J.; Morante, J. R.; Juli, M. A.; Mathur, S.; Romano-Rodriguez, A. *Adv. Funct. Mater.* **2008**, *18*, 2990−2994.

(5) Vallejos, S.; Stoycheva, T.; Umek, P.; Navio, C.; Snyders, R.; Bittencourt, C.; Llobet, E.; Blackman, C.; Moniz, S.; Correig, X. *Chem. Commun.* **2011**, *47*, 565−567.

(6) Huh, J. H.; Joo, M. K.; Jang, D. Y.; Lee, J. H.; Kim, G. T. *J. Mater. Chem.* **2012**, *22*, 24012−24016.

(7) Li, Y. S.; Xu, J.; Chao, J. F.; Chen, D.; Ouyang, S. X.; Ye, J. H.; Shen, G. Z. *J. Mater. Chem.* **2011**, *21*, 12852−12857.

(8) Qiu, J. J.; Li, X. M.; Gao, X. D.; Weng, B. B.; Li, L.; Yuan, Z. J.; Shi, Z. S.; Hwang, Y. H. *J. Mater. Chem.* **2012**, *22*, 23411−23417.

(9) Faglia, G.; Baratto, C.; Sberveglieri, G.; Zha, M.; Zappettini, A. *Appl. Phys. Lett.* **2005**, *86*, 011923.

(10) Mattei, G.; Mazzoldi, P.; Post, M. L.; Buso, D.; Guglielmi, M.; Martucci, A. *Adv. Mater.* **2007**, *19*, 561−564.

(11) Korotcenkov, G.; Brinzari, V.; Stetter, J. R.; Blinov, I.; Blaja, V. *Sens. Actuators, B* **2007**, *128*, 51−63.

(12) Tamaekong, N.; Liewhiran, C.; Wisitoraat, A.; Phanichphant, S. *Sens. Actuators, B* **2011**, *152*, 155−161.

(13) Xue, X. Y.; Xing, L. L.; Chen, Y. J.; Shi, S. L.; Wang, Y. G.; Wang, T. H. *J. Phys. Chem. C* **2008**, *112*, 12157−12160.

(14) Tien, L. C.; Sadik, P. W.; Norton, D. P.; Voss, L. F.; Pearton, S. J.; Wang, H. T.; Kang, B. S.; Ren, F.; Jun, J.; Lin. *J. Appl. Phys. Lett.* **2005**, *87*, 222106.

(15) Kolmakov, A.; Kienov, D. O.; Liach, Y.; Stemmer, S.; Moskovits, M. *Nano Lett.* **2005**, *5*, 667−673.

(16) Cheng, C. W.; Liu, B.; Yang, H. Y.; Zhou, W. W.; Sun, L.; Chen, R.; Yu, S. F.; Zhang, J. X.; Gong, H.; Sun, H. D.; Fan, H. J. *ACS Nano* **2009**, *3*, 3069−3076.

(17) Bierman, M. J.; Jin, S. *Energy Environ. Sci.* **2009**, *2*, 1050−1059.

(18) Fang, C.; Geng, B.; Liu, J.; Zhan, F. *Chem. Commun.* **2009**, 2350−2352.

(19) Chen, Z. G.; Cheng, L.; Xu, H. Y.; Liu, J.; Zou, Z. J.; Sekiguchi, T.; Lu, G. Q.; Cheng, H. M. *Adv. Mater.* **2010**, *22*, 2376−2380.

(20) Li, G. H.; Zhai, T. Y.; Jiang, Y.; Bando, Y.; Golberg, D. *J. Phys. Chem. C* **2011**, *115*, 9740−9745.

(21) Choi, S. W.; Katoch, A.; Sun, G. J.; Kim, S. S. *Sens. Actuators, B* **2013**, *181*, 787−794.

(22) Ahmed, M. A.; El-Katori, E. E.; Gharni, Z. H. *J. Alloys Compd.* **2013**, *553*, 19−29.

(23) Yu, L.; Wang, Z. Y.; Zhang, L.; Wu, H. B.; Lou, X. W. *J. Mater. Chem. A* **2013**, *122*, 122−127.

(24) Cui, B.; Peng, H. X.; Xia, H. Q.; Guo, X. H.; Guo, H. L. *Sep. Purif. Technol.* **2013**, *103*, 251−257.

(25) Zhu, C. L.; Yu, H. L.; Zhang, Y.; Wang, T. S.; Ouyang, Q. Y.; Qi, L. H.; Chen, Y. J.; Xue, X. Y. *ACS Appl. Mater. Interfaces* **2012**, *4*, 665−671.

(26) Deng, J. N.; Yu, B.; Lou, Z.; Wang, L. L.; Wang, R.; Zhang, T. *Sens. Actuators, B* **2013**, *184*, 21−26.

(27) Wang, H. G.; Fei, X. L.; Wang, L.; Li, Y.; Xu, S. F.; Sun, M. D.; Sun, L.; Zhang, C. Q.; Li, Y. P.; Yang, Q. B.; Wei, Y. *New J. Chem.* **2011**, *35*, 1795−1802.

(28) Song, P.; Wang, Q.; Yang, Z. X. *Sens. Actuators, B* **2012**, *168*, 421−428.

(29) Wang, L. L.; Dou, H. M.; Lou, Z.; Zhang, T. *Nanoscale* **2013**, *5*, 2686−2691.

(30) Yang, R.; Huang, X.; Wang, Z. Y.; Zhou, Y. Z.; Liu, L. T. *Sens. Actuators, B* **2010**, *145*, 474−479.

(31) Zou, B.; Wu, F. Q.; Chen, C.; Ren, H.; Wang, Z. Y.; Zou, L. H. *Sens. Actuators, B* **2006**, *119*, 370−373.

(32) Huang, L. M.; Fan, H. Q. *Sens. Actuators, B* **2012**, *171−172*, 1257−1263.

(33) Cho, Y. H.; Kang, Y. C.; Lee, J. H. *Sens. Actuators, B* **2013**, *176*, 971−977.

(34) Roy, S.; Basu, S. *J. Mater. Sci. Mater. Electron.* **2004**, *15*, 321−326.

(35) Tong, M.; Dai, G.; Gao, D. S. *Mater. Chem. Phys.* **2001**, *69*, 176−179.

(36) Lu, X. F.; Yu, Q. Q.; Wang, K.; Shi, L. C.; Liu, X.; Qiu, A. G.; Wang, L.; Cui, D. L. *Cryst. Res. Technol.* **2010**, *45*, 557−561.

(37) Bekermann, D.; Gasparotto, A.; Barreca, D.; Maccato, C.; Comini, E.; Sada, C.; Sberveglieri, G.; Devi, A.; Fischer, R. A. *ACS Appl. Mater. Interfaces* **2012**, *4*, 928−934.

(38) Niu, M. T.; Huang, F.; Cui, L. F.; Huang, P.; Yu, Y. L.; Wang, Y. S. *ACS Nano* **2010**, *4*, 681−688.

(39) Chen, Y. J.; Xiao, G.; Wang, T. S.; Zhang, F.; Ma, Y.; Gao, P.; Zhu, C. J.; Zhang, E.; Xu, Z.; Li, Q. H. *Sens. Actuators, B* **2011**, *156*, 867−874.

(40) Patil, L. A.; Shinde, M. D.; Bari, A. R.; Deo, V. V.; Patil, D. M.; Kaushik, M. K. *Sens. Actuators, B* **2011**, *155*, 174−182.

(41) Khoang, N. D.; Trung, D. D.; Duy, N. V.; Hoa, N. D.; Hieu, N. V. *Sens. Actuators, B* **2012**, *174*, 594−601.

(42) Wang, Z. L. *Ann. Rev. Phys. Chem.* **2004**, *55*, 159−196.

(43) Sysoev, V. V.; Goschnick, J.; Schneider, T.; Strelcov, E.; Kolmakov, A. *Nano Lett.* **2007**, *7*, 3182−3188.